organics

MDPI

Article

Frontier Orbitals and Charges Approaches in Electrophilic Aromatic Substitution: The Cases of Anisole and Benzaldehyde

Lucia Emanuele [1], Rocco Racioppi [2] and Maurizio D'Auria [2,*]

[1] Department of Arts and Restoration, University of Dubrovnik, Branitelja Dubrovnika 41, 20000 Dubrovnik, Croatia; l.emanuel@unidu.hr
[2] Dipartimento di Scienze di Base ed Applicate, Università della Basilicata, via dell'Ateneo Lucano 10, 85100 Potenza, Italy; rocco.racioppi@unibas.it
* Correspondence: maurizio.dauria53@gmail.com

Abstract

The study aimed to verify the possible use of DFT calculation in the prediction of the orientation in electrophilic aromatic substitution. An activated ortho/para orienting substrate, and a deactivated meta orienting substrate, were used in DFT calculations using B3LYP, B3PW91, BPV86, CAM-B3LP, HCTH, HSEH1PBE, LSDA, MPW1PW91, PBEPBE, TPSSTPSS, and WB97XD functionals. The results showed that the reactivity of anisole can be adequately described considering charge control in reaction performed in hard conditions (nitration), while frontier orbital control can play a role in reactions performed in softer conditions (chlorination). Nitration of benzaldehyde can be rationalized through Hirshfeld charges analysis. Neither the frontier orbital nor Mulliken charges approach adequately account for behavior observed in chlorination of benzaldehyde. The effect of different basis sets was tested performing calculations with B3LYP functional and aug-cc-pVDZ, 6-311G+(d,p), aug-cc-pVQZ, DGTZVP, and LanL2DZ basis sets. For anisole, all basis sets provided a HOMO electron density distribution consistent with experimental reactivity; Hirshfeld charges analysis consistently reproduced the observed reactivity of anisole across all tested basis sets. All the basis sets were able to explain the observed reactivity of benzaldehyde in hard experimental condition, while they failed to give a correct description when a softer reagent was used.

Keywords: aromatic compounds; electrophilic substitution; frontier orbitals control; Mulliken charges; Hirshfeld charges

1. Introduction

Electrophilic aromatic substitutions are some of the most studied reactions in organic chemistry. In 1874, Koerner determined the regioselective effects of the substituents in mono-, bi-, and trisubstituted aromatic rings [1]. A first explanation of the substituent effects on the regioselectivity of electrophilic aromatic substitutions has been described considering the alternating polarity theory [2]. In 1942, Wheland proposed the formation of an arenium ion as an intermediate [3]. The mechanism of the electrophilic aromatic substitution was explained on the basis of this intermediate [4]. The mechanism of electrophilic aromatic substitution was the basis of several theoretical approaches able to explain the regioselectivity of the reaction. DFT treatment of the mechanism has been published [5,6], and several other contributions in this field appeared [7–13]. Fukui's 1952 pioneering work introduced frontier molecular orbital (FMO) theory by showing that the regions of highest electron density in the HOMO of polycyclic aromatic hydrocarbons, calculated using

Check for updates

Academic Editor: Wim Dehaen

Received: 30 January 2026
Revised: 21 February 2026
Accepted: 26 February 2026
Published: 4 March 2026

Copyright: © 2026 by the authors. Licensee MDPI, Basel, Switzerland. This article is an open access article distributed under the terms and conditions of the Creative Commons Attribution (CC BY) license.

LCAO-MO methods and symmetry considerations, predict the sites most susceptible to electrophilic attack [14–16]. Some years later, Klopman and Salem proposed a general approach to explain perturbation of the energy of a reactive system based on both the interaction between the orbitals of the reagents and the interaction between charges [17–19]. In 2014, the regioselectivity of aromatic substitutions was attributed to charge redistribution within the benzene ring, rather than to the electron-donating or electron-withdrawing nature of substituents [20]. Recently, we reported the results of DFT calculations (B3LYP/aug-cc-pVDZ level of approximation) on the electrophilic aromatic substitution. Our analysis shows that the frontier orbital control and/or the charge control can be applied to explain the reactivity of activated *ortho*/*para*-orienting compounds, depending on the nature of the electrophile. On the contrary, both approaches failed in the description of the reactivity of deactivated *meta*-orienting substrates [21]. This article aims to determine whether the limitations observed in the previous study arise from the selected systems or the computational conditions by comparing anisole, an activated *ortho*/*para*-directing substrate, with benzaldehyde, a deactivated *meta*-directing substrate, and analyzing the results obtained with different functionals and basis sets. In this article, we want to verify if Klopman–Salem approach performed at DFT stadium is able to describe the regiochemical behavior in electrophilic aromatic substitutions. To perform this study, we calculated the HOMO (highest occupied molecular orbital) and the NHOMO (next occupied molecular orbital), if necessary, of the substrates, as well as the Hirshfeld [22] and Mulliken charges [23]. Hirshfeld charges can be considered one of the best method to describe charge population in a molecule [24] and have been used to discuss electrophilic aromatic substitutions [16], although the method seems to fail in some cases [25].

2. Materials and Methods

Gaussian09 has been used for discussions about computed geometries [26]. All the computations were based on the Density Functional Theory (DFT) by using the B3LYP hybrid xc functional [27], B3PW91 [28], BPV86 [29], CAM-B3LYP [30], HCTH [31], HSEH1PBE [32–38], LSDA [39], MPW1PW91 [40], PBEPBE [41], TPSSTPSS [42,43], and WB97XD [44]. Geometry optimizations from the Gaussian09 program have been obtained at aug-cc-pVDZ [45], 6-311G+(d,p) [46], aug-cc-pVQZ [47], DGTZVP [48], and LanL2DZ [49] level of approximation. Geometry optimizations were performed with default settings on geometry convergence (gradients and displacements), integration grid and electronic density (SCF) convergence. Redundant coordinates were used for geometry optimization as produced by the Gaussian09 program. Analytical evaluation of the energy second derivative matrix with regard to Cartesian coordinates (Hessian matrix) confirmed the nature of minima on the energy surface points associated with the optimized structures. Z-matrix of the optimized structures are reported in Supplementary Materials.

3. Results

The first series of calculations were performed using all the different functionals (see Section 2) with the same basis set (aug-cc-pVDZ). The results for anisole are reported in Table 1 and Figure 1. To better interpret these results, we compared them with experimental reactivity. We considered two representative electrophilic substitution reactions: nitration, typically carried out under harsh experimental conditions, and chlorination, which proceeds under milder conditions. Experimentally, nitration of anisole yields 44% *o*-nitroanisole and 56% *p*-nitroanisole, while chlorination gives 21% *o*-chloroanisole and 79% *p*-chloroanisole [50]. When B3LYP functional was used, the HOMO was found at −6.92 eV. The electron density was higher in *ortho* (0.036) and *para* position (0.109) than in *meta* position (0.023). These results agree with those obtained in the chlorination reaction,

where the attack in *para* position was favored. Although the results were similar regardless of the functional, with some of them (BPV96, HCTH, LSDA, PBEPBE, TPSSTPSS), the difference in electron density between the ortho and para positions was smaller than with B3LYP functional.

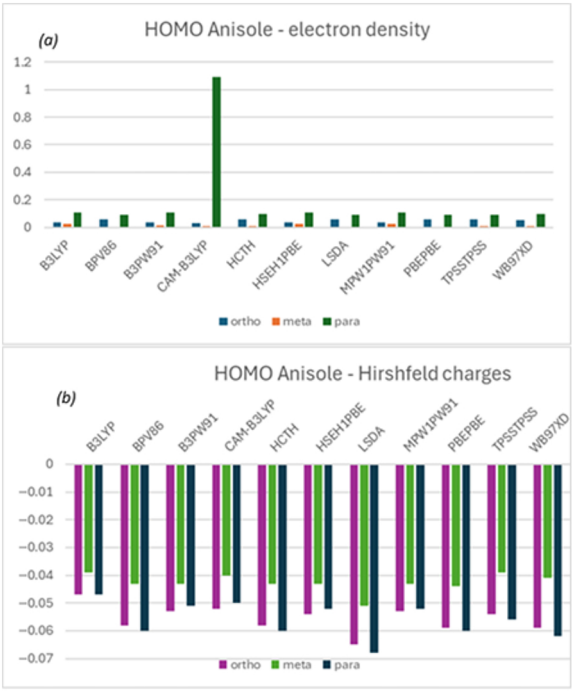


Figure 1. (**a**) Electron densities on HOMO and (**b**) Hirshfeld charges of anisole obtained using different functionals.

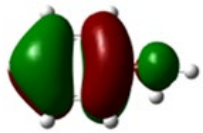
Mulliken charges did not agree with the experimental results when B3LYP functional was used, as all the carbon atoms on the aromatic ring showed a positive charge. The smallest charge (0.72) was in *para* position, consistent with the prevalence of *para* isomer in the reactions; however, *ortho* position showed the highest positive charge, which does not align with experimental practice. When other functionals were used, different results were obtained. The B3PW91, BPV86, HCTH, HSEH1PBE, MPW1PW91, PBEPBE, TPSSTPSS, and WB97XD functionals showed that all the carbon atoms on the aromatic ring were positive, but the highest positive charges were in the *meta* position in agreement with *ortho-para* orientation. However, with the other functionals (HCTH, PBEPBE, TPSSTPSS, and WB97XD), the positive charge in *para* position was higher than in *ortho*, indicating a preference for a reaction on this position, not in agreement with the experimental results.

Hirshfeld charges calculated with the B3LYP functional showed a negative charge on all the atoms in the ring, with the highest negative charges in the *ortho* and *para* position. This result aligns particularly well with experimental data from nitration, where the yields of *o*- and *p*-nitroanisole were quite similar. This behavior indicates that charges play a significant role in determining the orientation during nitration. The same pattern was confirmed using all other functionals: in every case, all carbon atoms on the aromatic ring showed negative charges, with the highest negative charges in the *ortho* and *para* position. However, in some cases (B3PW91, CAM-B3LYP, HSEH1PBE, and MPW1PW91) the charges in the *ortho* positions were higher than those in the *para* position, indicating a preference for the attack in the *ortho* position not in agreement with the experimental results.

Table 1. Atomic coefficients, electronic densities on HOMO, Mulliken charges, and Hirshfeld charges of anisole obtained using different functionals.

Functional	HOMO					Mulliken Charges			Hirshfeld Charges		
	Energy [eV]	Atomic Coefficients Electron Density									
		ortho	*meta*	*para*	*ortho*	*meta*	*para*	*ortho*	*meta*	*para*
B3LYP	−6.92	0.19 0.036	−0.15 0.023	−0.33 0.109	0.90	0.87	0.72	−0.047	−0.039	−0.047
BPV86	−5.47	−0.24 0.058	0.07 0.005	0.30 0.09	0.43	0.79	0.45	−0.058	−0.043	−0.060
B3PW91	−6.83	0.19 0.036	−0.11 0.012	−0.33 0.109	0.64	0.78	0.51	−0.053	−0.043	−0.051
CAM-B3LYP	−8.22	0.18 0.032	−0.10 0.01	−0.33 1.09	0.92	0.88	0.69	−0.052	−0.040	−0.050
HCTH	−5.53	0.24 0.058	0.08 0.006	0.31 0.096	0.14	1.00	0.39	−0.058	−0.043	−0.060
HSEH1PBE	−6.62	−0.19 0.036	0.15 0.023	0.33 0.109	0.62	0.79	0.51	−0.054	−0.043	−0.052

Table 1. *Cont.*

Functional	HOMO					Mulliken Charges			Hirshfeld Charges		
	Energy [eV]	Atomic Coefficients Electron Density									
LSDA		−6.06	−0.24 0.058	0.05 0.003	0.30 0.09	0.67	0.56	0.49	−0.065	−0.051	−0.068
MPW1PW91		−7.02	−0.19 0.036	0.15 0.023	0.33 0.109	0.60	0.76	0.48	−0.053	−0.043	−0.052
PBEPBE		−5.39	−0.24 0.058	0.07 0.005	0.30 0.09	0.36	0.82	0.42	−0.059	−0.044	−0.060
TPSSTPSS		−5.35	−0.24 0.058	0.08 0.006	0.30 0.09	0.25	0.82	0.35	−0.054	−0.039	−0.056
WB97XD		−8.16	−0.23 0.053	0.08 0.006	0.31 0.096	0.37	0.72	0.41	−0.059	−0.041	−0.062

Considering the above reported results, the best representation of the actual reactivity of anisole can be obtained by using BPV86, PBEPBE, TPSSTPSS, and WB97XD functionals.

Table 2 and Figure 2 show the optimization results for benzaldehyde with different functionals. As in the previous case, the frontier orbital and charge analyses must be compared with experimental data. Nitration predominantly afforded *m*-nitrobenzaldehyde in 80% yields [51], while the direct chlorination of benzaldehyde gave a mixture of *meta* and *para* isomers [52]. However, direct chlorination is rarely employed for the synthesis of *m*-chlorobenzaldehyde, which is more efficiently obtained via a Sandmeyer reaction starting from *m*-nitrobenzaldehyde. Most of the functionals indicated that the HOMO was an n orbital, localized mainly on the oxygen atom; only CAM-B3LYP and WB97XD gave a π orbital as HOMO. Consequently, the discussion on frontier orbital control was performed on considering NHOMO (next highest occupied molecular orbital). NHOMO is not meaningful as a reactive orbital. For the B3LYP, BPV86, HCTH, MPW1PW91, PBEPBE, and TPSSTPSS functionals, the highest electron densities were found in the *meta* and *ortho* positions, usually with similar values at both positions. This prediction, however, is not consistent with experimental observations. The B3PW91 functional localized the highest electron density only on a single carbon in the *meta* position, while the HSEH1PBE functional localized the highest electron density on one carbon in the *ortho* position. The CAM-B3LYP and WB97XD functionals predicted high electron density not only at the *meta* and *ortho* positions, but they were the only functionals to indicate also a possible attack in *para*. However, the attack in *ortho* has not be described. Overall, the frontier orbital approach failed to rationalize the experimental reactivity of benzaldehyde.

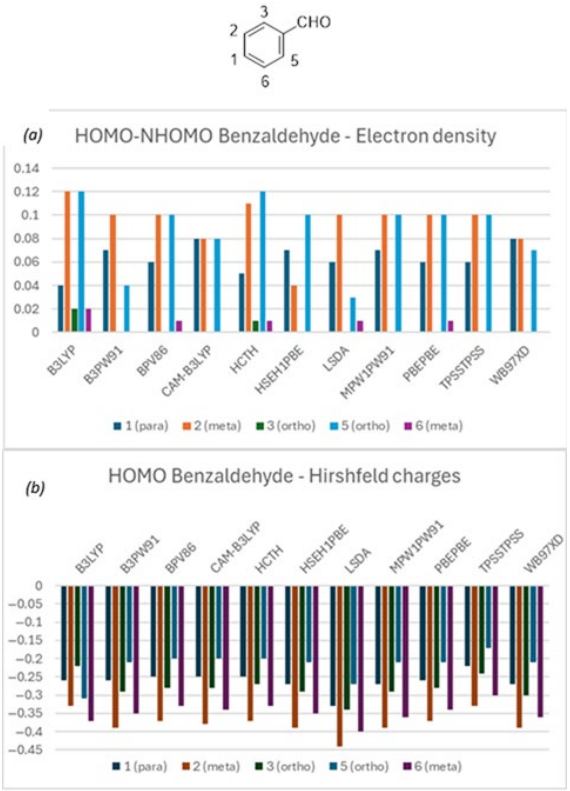
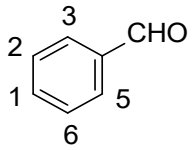


Figure 2. (**a**) Electron densities on HOMO and (**b**) Hirshfeld charges of benzaldehyde obtained using different functionals.

Table 2. Atomic coefficients, electronic densities on HOMO, Mulliken charges, and Hirshfeld charges of benzaldehyde obtained using different functionals.



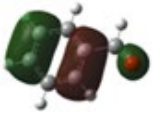
Functional	Frontier Orbitals								Mulliken Charges					Hirshfeld Charges [x10]				
	HOMO	NHOMO	Energy [eV]	Atomic Coefficients Electron Density														
				1 (*p*)	2 (*m*)	3 (*o*)	5 (*o*)	6 (*m*)	1 (*p*)	2 (*m*)	3 (*o*)	5 (*o*)	6 (*m*)	1 (*p*)	2 (*m*)	3 (*o*)	5 (*o*)	6 (*m*)
B3LYP			−7.36						0.42	0.63	0.55	0.45	0.58	−0.26	−0.33	−0.22	−0.31	−0.37
			−7.49	−0.19 0.04	−0.34 0.12	−0.14 0.02	0.34 0.12	0.15 0.02										
B3PW91			−7.27						0.30	0.37	0.33	0.43	0.46	−0.26	−0.39	−0.29	−0.21	−0.35
			−7.58	0.26 0.07	0.31 0.10	0.03 0.00	−0.19 0.04	−0.03 0.00										
BPV86			−6.02						0.39	0.42	0.42	0.59	0.50	−0.25	−0.37	−0.28	−0.20	−0.33
			−6.85	−0.25 0.06	−0.32 0.10	−0.07 0.00	0.32 0.10	0.08 0.01										
CAM-B3LYP			−8.93	−0.29 0.08	−0.29 0.08	0.01 0.00	0.28 0.08	0.00 0.00	0.48	0.48	0.47	0.64	0.57	−0.25	−0.38	−0.28	−0.20	−0.34

Table 2. *Cont.*

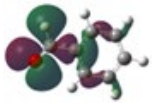
Functional	Frontier Orbitals								Mulliken Charges					Hirshfeld Charges [x10]				
	HOMO	NHOMO	Energy [eV]	Atomic Coefficients Electron Density														
				1 (*p*)	2 (*m*)	3 (*o*)	5 (*o*)	6 (*m*)	1 (*p*)	2 (*m*)	3 (*o*)	5 (*o*)	6 (*m*)	1 (*p*)	2 (*m*)	3 (*o*)	5 (*o*)	6 (*m*)
HCTH			−6.10						0.37	0.55	0.31	0.51	0.65	−0.25	−0.37	−0.27	−0.20	−0.33
			−6.93	−0.23 0.05	−0.33 0.11	−0.10 0.01	0.34 0.12	0.11 0.01										
HSEH1PBE			−7.13						0.31	0.37	0.32	0.42	0.48	−0.27	−0.39	−0.29	−0.21	−0.35
			−7.35	0.26 0.07	0.19 0.04	0.05 0.00	−0.31 0.10	−0.06 0.00										
LSDA			−6.53						0.42	0.25	0.40	0.57	0.36	−0.33	−0.44	−0.34	−0.27	−0.40
			−7.50	−0.25 0.06	−0.32 0.10	−0.06 0.00	0.17 0.03	0.08 0.01										
MPW1PW91			−7.58						0.28	0.35	0.30	0.38	0.45	−0.27	−0.39	−0.29	−0.21	−0.36

Table 2. *Cont.*

Functional	Frontier Orbitals								Mulliken Charges					Hirshfeld Charges [x10]				
	HOMO	NHOMO	Energy [eV]	Atomic Coefficients Electron Density														
				1 (*p*)	2 (*m*)	3 (*o*)	5 (*o*)	6 (*m*)	1 (*p*)	2 (*m*)	3 (*o*)	5 (*o*)	6 (*m*)	1 (*p*)	2 (*m*)	3 (*o*)	5 (*o*)	6 (*m*)
			−7.76	0.26 0.07	0.31 0.10	0.04 0.00	−0.31 0.10	−0.05 0.00										
PBEPBE			−5.91						0.38	0.42	0.38	0.57	0.51	−0.26	−0.37	−0.28	−0.21	−0.34
			−6.78	−0.25 0.06	−0.32 0.10	−0.07 0.00	0.32 0.10	0.08 0.01										
TPSSTPSS			−5.98						0.30	0.41	0.31	0.41	0.50	−0.22	−0.33	−0.24	−0.17	−0.30
			−6.72	−0.25 0.06	−0.32 0.10	−0.06 0.00	0.32 0.10	0.07 0.00										
WB97XD			−9.48	−0.29 0.08	−0.28 0.08	0.02 0.00	0.27 0.07	−0.01 0.00	0.34	0.37	0.37	0.46	0.46	−0.27	−0.39	−0.30	−0.21	−0.36

Mulliken charges analysis also proved inadequate to describe the substrate's reactivity. With B3LYP, B3PW91, BPV86, and WB97XD functionals, the lowest positive charge (all aromatic carbons being positively charged) was found in the *para* position. CAM-B3LYP indicated the lowest positive charge in both *para* and *meta* positions, in agreement with the chlorination experimental behavior but inconsistent with nitration results. HCTH predicted the lowest positive charges in the *ortho* position, LSDA functional at a single carbon atom in *meta* position, and HSEH1PBE, MPW1PW91, PBEPBE, and TPSSTPSS functionals at both *para* and *ortho* positions. On the contrary, Hirshfeld charges provided a more reliable description under harsh experimental conditions, such as nitration: in all tested functionals, the carbon atoms at the *meta* positions carried the highest negative charges.

In conclusion, the nitration of benzaldehyde can be rationalized through Hirshfeld charges analysis, which supports a charge-controlled mechanism. By contrast, neither the frontier orbital nor Mulliken charges approach adequately account for the chemical behavior observed in the chlorination of benzaldehyde.

After testing different functionals, we evaluated the effect of the basis set on the results. Table 3 and Figure 3 collect the results of calculations performed on anisole using the B3LYP functional with aug-cc-pVDZ [45], 6-311G+(d,p) [46], aug-cc-pVQZ [47], DGTZVP [48], and LanL2DZ [49] basis sets. Some significant differences emerged. All basis sets provided a HOMO electron density distribution consistent with experimental reactivity, with the highest values at the *ortho* and *para* positions. Mulliken charges analysis, however, proved inadequate to rationalize reactivity. Interestingly, aug-cc-pVDZ gave only positive charges on the aromatic carbons, whereas the other basis sets predicted negative charges. Among these, 6-311G+(d,p) gave the highest negative charges in the *para* and *meta* positions, aug-cc-pVQZ in the *meta* positions, and both DGTZVP and LanL2DZ in *ortho* positions. On the contrary, Hirshfeld charges analysis consistently reproduced the observed reactivity of anisole across all tested basis sets.

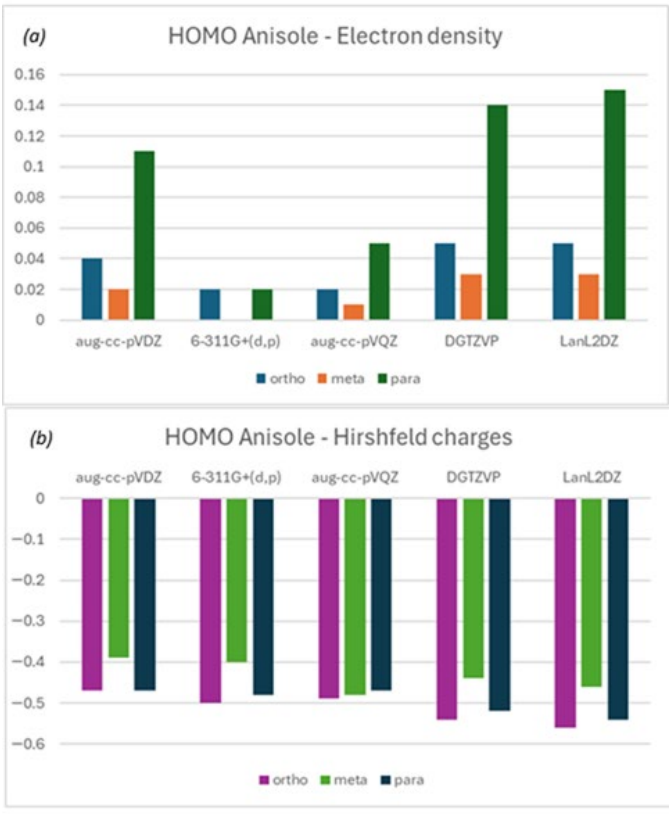
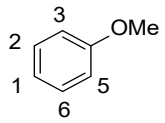
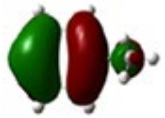


Figure 3. (**a**) Electron densities on HOMO and (**b**) Hirshfeld charges of anisole obtained using different basis sets with B3LYP functional.

Table 3. Atomic coefficients, electronic densities on HOMO, Mulliken charges, and Hirshfeld charges of anisole obtained using different basis sets with B3LYP functional.



Basis Set	Frontier Orbital							Mulliken Charges					Hirshfeld Charges [x10]				
	HOMO	Energy [eV]	Atomic Coefficients Electron Density														
			1 (*p*)	2 (*m*)	3 (*o*)	5 (*o*)	6 (*m*)	1 (*p*)	2 (*m*)	3 (*o*)	5 (*o*)	6 (*m*)	1 (*p*)	2 (*m*)	3 (*o*)	5 (*o*)	6 (*m*)
aug-cc-pVDZ		−6.92	−0.33 0.11	−0.15 0.02	0.19 0.04	0.19 0.04	−0.15 0.02	0.72	0.87	0.90	0.90	0.87	−0.47	−0.39	−0.47	−0.47	−0.39
6-311G+(d,p)		−6.81	−0.15 0.02	−0.07 0.00	0.13 0.02	0.13 0.02	−0.07 0.00	−0.14	−0.17	0.05	0.05	−0.17	−0.48	−0.40	−0.50	−0.51	−0.40
aug-cc-pVQZ		−6.81	0.22 0.05	0.10 0.01	−0.13 0.02	−0.13 0.02	0.10 0.01	−0.43	−0.51	−0.47	−0.47	−0.51	−0.47	−0.38	−0.45	−0.49	−0.48
DGTZVP		−6.72	−0.38 0.14	−0.17 0.03	0.22 0.05	0.22 0.05	−0.17 0.03	−0.24	−0.20	−0.34	−0.34	−0.20	−0.52	−0.44	−0.54	−0.54	−0.44
LanL2DZ		−6.65	−0.39 0.15	−0.17 0.03	0.23 0.05	0.23 0.05	−0.17 0.03	−0.24	−0.18	−0.35	−0.35	−0.18	−0.54	−0.46	−0.56	−0.56	−0.46

https://doi.org/10.3390/org7010013

The results obtained for benzaldehyde with different basis sets are reported in Table 4 and Figure 4. For all basis sets, the HOMO was identified as a *n* orbital, unable to give an electrophilic aromatic substitution; thus, the NHOMO was considered as the relevant frontier orbital. With aug-cc-pVDZ, the highest electron densities were found in the *ortho* and *meta* positions, while 6-311G+(d,p) and aug-cc-pVQZ gave similar results but localized on different carbons. DGTZVP and LanL2DZ predicted the highest electron densities across all aromatic carbons. Mulliken charges again failed to account for substitution patterns: 6-311G+(d,p) basis set gave the highest negative charge in the *ortho* position, aug-cc-pVQZ in the *para* and *meta* positions, and both DGTVP and LanL2DZ basis sets in the *ortho* positions. On the other side, all the basis sets provided a consistent explanation of benzaldehyde reactivity under harsh experimental conditions, giving the highest negative charges in *meta* positions.

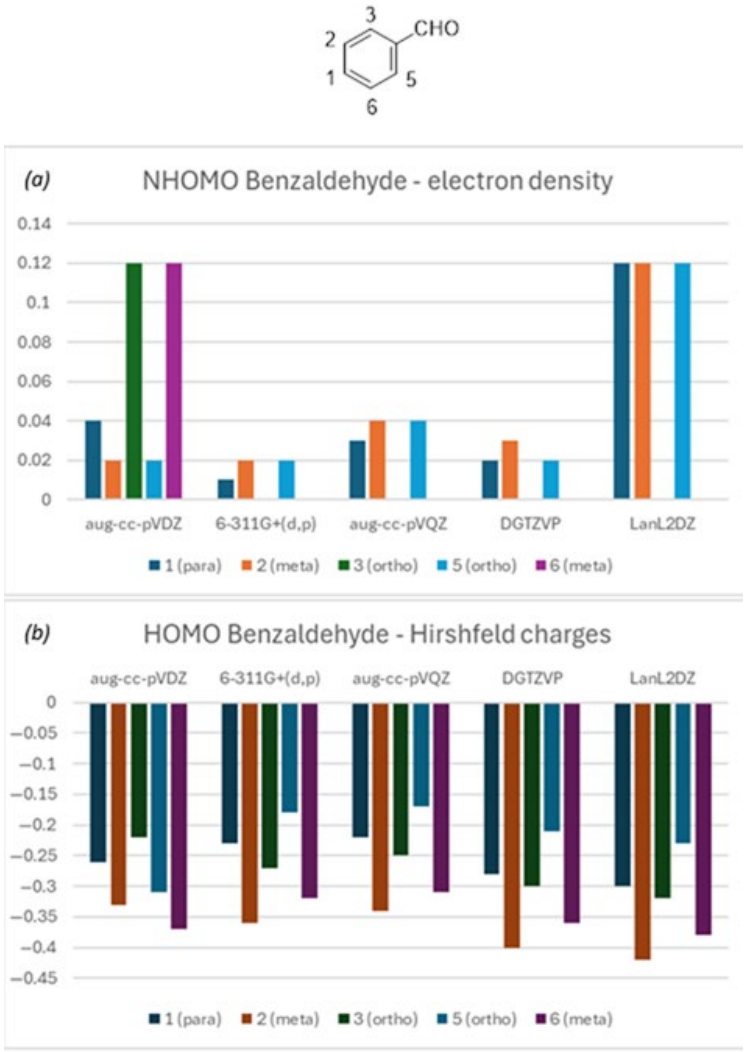
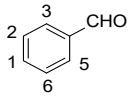


Figure 4. (**a**) Electron densities on NHOMO and (**b**) Hirshfeld charges of benzaldehyde obtained.

Table 4. Atomic coefficients, electronic densities on HOMO and NHOMO, Mulliken charges, and Hirshfeld charges of benzaldehyde obtained using different basis sets with B3LYP functional.



Basis Set	Frontier Orbitals								Mulliken Charges					Hirshfeld Charges [x10]				
	HOMO	NHOMO	Energy [eV]	Atomic Coefficients Electron Density														
				1 (*p*)	2 (*m*)	3 (*o*)	5 (*o*)	6 (*m*)	1 (*p*)	2 (*m*)	3 (*o*)	5 (*o*)	6 (*m*)	1 (*p*)	2 (*m*)	3 (*o*)	5 (*o*)	6 (*m*)
aug-cc-pVDZ			−7.36						0.42	0.63	0.55	0.45	0.58	−0.26	−0.33	−0.22	−0.31	−0.37
			−7.49	−0.19 0.04	0.15 0.02	0.34 0.12	−0.14 0.02	−0.34 0.12										
6-311G+(d,p)			−7.34						−0.12	−0.13	−0.70	−0.08	−0.16	−0.23	−0.36	−0.27	−0.18	−0.32
			−7.55	0.11 0.01	0.14 0.02	0.02 0.00	−0.14 0.02	−0.03 0.00										
aug-cc-pVQZ			−7.31						−0.45	−0.41	−0.25	−0.18	−0.44	−0.22	−0.34	−0.25	−0.17	−0.31
			−7.56	0.17 0.03	0.21 0.04	0.04 0.00	−0.21 0.04	−0.04 0.00										
DGTZVP			−7.27						−0.22	−0.22	−0.32	−0.30	−0.21	−0.28	−0.40	−0.30	−0.21	−0.36
			−7.47	0.14 0.02	0.16 0.03	0.02 0.00	−0.15 0.02	−0.03 0.00										
LanL2DZ			−7.15						−0.21	−0.21	−0.36	−0.34	−0.20	−0.30	−0.42	−0.32	−0.23	−0.38
			−7.42	−0.34 0.12	−0.35 0.12	0.00 0.00	0.34 0.12	0.01 0.00										

4. Conclusions

DFT calculations on anisole and benzaldehyde gave different and problematic results. Generally, the calculation results were able to explain the chemical reactivity of anisole, an activate *ortho*/*para* orienting compound, showing that, in hard experimental conditions such as in the nitration reaction, the reactivity is determined by the charges, calculated as Hirshfeld charges. When softer experimental conditions were used, such in in the chlorination reaction, the contribution of frontier orbitals could not be excluded.

Different behaviors were observed when benzaldehyde was considered. In this case, the reactivity in hard experimental conditions could be described by using Hirshfeld charges, while frontier orbital interactions could not be invoked in order to justify the reactivity of the substrate in soft experiments.

The above reported results confirmed that the Klopman–Salem approach has to be used with appropriate precautions in the description of the electrophilic aromatic substitutions. A possible next step of this study could be the identification of the use of this approach on the reactivity of condensed aromatic molecules and to justify the divergent reactivity of benzofuran and indole.

Supplementary Materials: The following supporting information can be downloaded at: https://www.mdpi.com/article/10.3390/org7010013/s1, Z matrix of calculated compounds.

Author Contributions: Conceptualization, M.D. and L.E.; validation, R.R.; investigation, L.E. All authors have read and agreed to the published version of the manuscript.

Funding: This research received no external funding.

Data Availability Statement: Data are available in Supplementary Materials.

Conflicts of Interest: The authors declare no conflicts of interest.

References

1. Koerner, W. Studi sull'isomeria delle così dette sostanze aromatiche a sei atomi di carbonio. *Gazz. Chim. Ital.* **1874**, *4*, 305–446.
2. Karrer, P. *Lehrbuch der Organishen Chemie*; Georg Thieme Verlag: Stuttgart, Germany, 1963.
3. Wheland, G.W. A quantum mechanical investigation of the orientation of substitution in aromatic molecules. *J. Am. Chem. Soc.* **1942**, *64*, 900–908. [CrossRef]
4. Olah, G.A. Aromatic substitution. XXVIII. Mechanism of electrophilic aromatic substitutions. *Acc. Chem. Res.* **1971**, *4*, 240–248. [CrossRef]
5. Stuyver, T.; Danovich, D.; De Proft, F.; Shaik, S. Electrophilic aromatic substitution reactions: Mechanistic landascape, electrostatic and electric-field control of reaction rates, and mechanistic crossovers. *J. Am. Chem. Soc.* **2019**, *141*, 9719–9730. [CrossRef]
6. Galabov, B.; Nalbantova, D.; Schleyer, P.v.R.; Schaefer, H.F., III. Electrophilic aromatic substitution: New insights into an old class of reactions. *Acc. Chem. Res.* **2016**, *49*, 1191–1199. [CrossRef]
7. Domingo, L.R. Molecular Electron Density Theory: A Modern View of Reactivity in Organic Chemistry. *Molecules* **2016**, *21*, 1319. [CrossRef]
8. Freire de Queiroz, J.; Walkimar, D.M.; Carneiro, J.; Sabino, A.A.; Sparrapan, R.; Eberlin, M.N.; Esteves, P.M. Electrophilic Aromatic Nitration: Understanding Its Mechanism and Substituent Effects. *J. Org. Chem.* **2006**, *71*, 6192–6203. [CrossRef]
9. Schwabe, T.; Grimme, S. Theoretical Description of Substituent Effects in Electrophilic Aromatic Substitution Reactions. *Eur. J. Org. Chem.* **2008**, *2008*, 5928–5935. [CrossRef]
10. Fievez, T.; Pinter, B.; Geerlings, P.; Bickelhaupt, F.M.; De Proft, F. Regioselectivity in Electrophilic Aromatic Substitution: Insights from Interaction Energy Decomposition Potentials. *Eur. J. Org. Chem.* **2011**, *2011*, 2958–2968. [CrossRef]
11. Szatylowicz, H.; Jezuita, A.; Krygowski, T.M. Aromaticity: A story of 150 years of development. *Struct. Chem.* **2019**, *30*, 1519–1548.
12. Starmenkovic, N.; Ulrih, N.P.; Cerkovnik, J. An analysis of electrophilic aromatic substitution: A "complex approach". *Phys. Chem. Chem. Phys.* **2021**, *23*, 5051–5068. [CrossRef]
13. Martins, F.A.; Freitas, M.P. Myths and Truths About Electrophilic Aromatic Substitution: The Particular Case of Fluorobenzene. *J. Phys. Org. Chem.* **2026**, *39*, e70063. [CrossRef]
14. Fukui, K.; Yonezawa, T.; Shingu, H. A molecular orbital theory of reactivity of aromatic hydrocarbons. *J. Chem. Phys.* **1952**, *20*, 722–725. [CrossRef]

15. Seeman, J.I. Kenichi Fukui, Frontier Molecular Orbital Theory, and the Woodward-Hoffmann Rules. Part II. A Sleeping Beauty in Chemistry. *Chem. Rec.* **2022**, *22*, e202100300. [CrossRef]
16. Elliott, R.J.; Sackwild, V.; Richards, W.G. Quantitative frontier orbital theory: Part I. Electrophilic aromatic substitution. *J. Mol. Struct.* **1982**, *86*, 301–314. [CrossRef]
17. Klopman, G. Chemical reactivity and the concept of charge- and frontier-controlled reactions. *J. Am. Chem. Soc.* **1968**, *90*, 223–234. [CrossRef]
18. Salem, L. Intermolecular orbital theory of the interaction between conjugated systems. I. General theory. *J. Am. Chem. Soc.* **1968**, *90*, 543–552. [CrossRef]
19. Salem, L. Intermolecular orbital theory of the interaction between conjugated systems. II. Thermal and photochemical cycloaddition. *J. Am. Chem. Soc.* **1968**, *90*, 553–566. [CrossRef]
20. Liu, S. Where does the electron go? The nature of *ortho*/*para* and *meta* group directing in electrophilic aromatic substitution. *J. Chem. Phys.* **2014**, *141*, 194109. [CrossRef]
21. Emanuele, L.; D'Auria, M. Limitations of frontier orbital and charge approaches in the description of electrophilic aromatic substitution. *Organics* **2025**, *6*, 34. [CrossRef]
22. Hirshfeld, F.L. Bonded-atom fragments for describing molecular charge densities. *Theor. Chim. Acta* **1977**, *44*, 129–138. [CrossRef]
23. Mulliken, R.S. Electronic population analysis on LCAO-MO molecular wave functions. *J. Chem. Phys.* **1955**, *23*, 1833–1840. [CrossRef]
24. Manz, T.A. Seven confluence principles: A case study of standardized statistical analysis for 26 methods that assign net atomic charges in molecules. *RSC Adv.* **2020**, *10*, 44121–44148. [CrossRef]
25. Saha, S.; Roy, R.K.; Ayers, P.W. Are the Hirshfeld and Mulliken population analysis schemes consistent with chemical intuition? *Int. J. Quantum Chem.* **2009**, *109*, 1790–1806. [CrossRef]
26. Frisch, M.J.; Trucks, G.W.; Schlegel, H.B.; Scuseria, G.E.; Robb, M.A.; Cheeseman, J.R.; Scalmani, G.; Barone, V.; Mennucci, B.; Petersson, G.A.; et al. *Gaussian 09, Revision A.1*; Gaussian, Inc.: Wallingford, CT, USA, 2009.
27. Becke, A.D. Density-functional thermochemistry. III. The role of exact exchange. *J. Chem. Phys.* **1993**, *98*, 5648–5652. [CrossRef]
28. Perdew, J.P.; Wang, Y. Accurate and simple analytic representation of the electron-gas correlation energy. *Phys. Rev. B* **1992**, *45*, 13244–13249. [CrossRef]
29. Perdew, J.P. Density-functional approximation for the correlation energy of the inhomogeneous electron gas. *Phys. Rev. B* **1986**, *33*, 8822−8824. [CrossRef] [PubMed]
30. Yanai, T.; Tew, D.; Handy, N. A new hybrid exchange-correlation functional using the Coulomb-attenuating method (CAM-B3LYP). *Chem. Phys. Lett.* **2004**, *393*, 51–57. [CrossRef]
31. Boese, A.D.; Handy, N.C. New exchange-correlation density functionals: The role of the kinetic-energy density. *J. Chem. Phys.* **2002**, *116*, 9559–9569. [CrossRef]
32. Heyd, J.; Scuseria, G. Efficient hybrid density functional calculations in solids: Assessment of the Heyd–Scuseria–Ernzerhof screened Coulomb hybrid functional. *J. Chem. Phys.* **2004**, *121*, 1187–1192. [CrossRef]
33. Heyd, J.; Scuseria, G.E. Assessment and validation of a screened Coulomb hybrid density functional. *J. Chem. Phys.* **2004**, *120*, 7274–7280. [CrossRef]
34. Heyd, J.; Peralta, J.E.; Scuseria, G.E.; Martin, R.L. Energy band gaps and lattice parameters evaluated with the Heyd-Scuseria-Ernzerhof screened hybrid functional. *J. Chem. Phys.* **2005**, *123*, 174101. [CrossRef]
35. Heyd, J.; Scuseria, G.E.; Ernzerhof, M. Hybrid functionals based on a screened Coulomb potential. *J. Chem. Phys.* **2003**, *118*, 8207–8215, Erratum in *J. Chem. Phys.* **2006**, *124*, 219906. https://doi.org/10.1063/1.2204597.
36. Henderson, T.M.; Izmaylov, A.F.; Scalmani, G.; Scuseria, G.E. Can short-range hybrids describe long-range-dependent properties? *J. Chem. Phys.* **2009**, *131*, 44108. [CrossRef]
37. Izmaylov, A.F.; Scuseria, G.E.; Frisch, M.J. Efficient evaluation of short-range Hartree-Fock exchange in large molecules and periodic systems. *J. Chem. Phys.* **2006**, *125*, 104103. [CrossRef]
38. Krukau, A.V.; Vydrov, O.A.; Izmaylov, A.F.; Scuseria, G.E. Influence of the exchange screening parameter on the performance of screened hybrid functionals. *J. Chem. Phys.* **2006**, *125*, 224106. [CrossRef] [PubMed]
39. Vosko, S.H.; Wilk, L.; Nusair, M. Accurate spin-dependent electron liquid correlation energies for local spin density calculations: A critical analysis. *Can. J. Phys.* **1980**, *58*, 1200–1211. [CrossRef]
40. Adamo, C.; Barone, V. Exchange functionals with improved long-range behavior and adiabatic connection methods without adjustable parameters: The *m*PW and *m*PW1PW models. *J. Chem. Phys.* **1998**, *108*, 664–675. [CrossRef]
41. Ernzerhof, M.; Perdew, J.P. Generalized gradient approximation to the angle- and system-averaged exchange hole. *J. Chem. Phys.* **1998**, *109*, 3313–3320. [CrossRef]
42. Tao, J.M.; Perdew, J.P.; Staroverov, V.N.; Scuseria, G.E. Climbing the Density Functional Ladder: Nonempirical Meta–Generalized Gradient Approximation Designed for Molecules and Solids. *Phys. Rev. Lett.* **2003**, *91*, 146401. [CrossRef]

43. Staroverov, V.N.; Scuseria, G.E.; Tao, J.; Perdew, J.P. Comparative assessment of a new nonempirical density functional: Molecules and hydrogen-bonded complexes. *J. Chem. Phys.* **2003**, *119*, 12129. [CrossRef]
44. Chai, J.-D.; Head-Gordon, M. Long-range corrected hybrid density functionals with damped atom–atom dispersion corrections. *Phys. Chem. Chem. Phys.* **2008**, *10*, 6615–6620. [CrossRef]
45. Dunning, T.H., Jr. Gaussian basis sets for use in correlated molecular calculations. I. The atoms boron through neon and hydrogen. *J. Chem. Phys.* **1989**, *90*, 1007–1023. [CrossRef]
46. Parr, R.G.; Yang, W. *Density Functional Theory of Atoms and Molecules*; Oxford University Press: Oxford, UK, 1989.
47. Peterson, K.A.; Woon, D.E.; Dunning, T.H., Jr. Benchmark calculations with correlated molecular wave functions. IV. The classical barrier height of the $H+H_2 \rightarrow H_2+H$ reaction. *J. Chem. Phys.* **1994**, *100*, 7410–7415. [CrossRef]
48. Godbout, N.; Salahub, D.R.; Andzelm, J.; Wimmer, E. Optimization of Gaussian-type basis sets for local spin density functional calculations. Part I. Boron through neon, optimization technique and validation. *Can. J. Chem.* **1992**, *70*, 560–571. [CrossRef]
49. Dunning, T.H., Jr.; Hay, P.J. Gaussian Basis Sets for Molecular Calculations. In *Modern Theoretical Chemistry*; Schaefer, H.F., III, Ed.; Plenum Press: New York, USA, 1977; Volume 3, pp. 1–28.
50. Stock, L.M. *Aromatic Substitution Reactions*; Prentice-Hall: Englewood Cliffs, NJ, USA, 1968; p. 63.
51. Davey, W.; Gwilt, J.R. The preparation of the mononitrobenzaldehydes. *J. Chem. Soc.* **1950**, 204–208. [CrossRef]
52. Erdmann, H.; Schwechten, E. Ueber gechlorte Abkömmlinge des Benzaldehyds. *Liebigs Ann. Chem.* **1890**, *260*, 53–78. [CrossRef]

Disclaimer/Publisher's Note: The statements, opinions and data contained in all publications are solely those of the individual author(s) and contributor(s) and not of MDPI and/or the editor(s). MDPI and/or the editor(s) disclaim responsibility for any injury to people or property resulting from any ideas, methods, instructions or products referred to in the content.